Carbohydrate Polymers 88 (2012) 618–627

Contents lists available at SciVerse ScienceDirect

Carbohydrate Polymers

journal homepage: www.elsevier.com/locate/carbpol

Effects of nanoliposomes based on soya, rapeseed and fish lecithins on chitosan thin films designed for tissue engineering

H.Y. Zhang [b], E. Arab Tehrany [a,*], C.J.F. Kahn [c,d], M. Ponçot [b], M. Linder [a], F. Cleymand [b]

[a] Laboratoire d'Ingénierie des Biomolécules, Nancy-Université, 2 Avenue de la Forêt de Haye, 54504 Vandoeuvre-Lès-Nancy Cedex, France
[b] Institut Jean Lamour, Ecole des Mines, Parc de Saurupt, CS 14234, 54042 Nancy, France
[c] LEMTA UMR7563, Nancy-Université, CNRS, 2 Avenue de la Forêt de Haye, BP 160, 54504 Vandoeuvre-Lès-Nancy Cedex, France
[d] Physiopathologie, Pharmacologie et Ingénierie Articulaires UMR7561, Nancy-Université, CNRS, 9 Avenue de la Forêt de Haye, BP 184, 54505 Vandoeuvre-Lès-Nancy, France

ARTICLE INFO

Article history:
Received 3 October 2011
Received in revised form 1 January 2012
Accepted 3 January 2012
Available online 11 January 2012

Keywords:
Functionalization
TH-AFM HarmoniX™ mode
Scaffold
Blend thin film

ABSTRACT

This work addresses the preparation of chitosan thin films functionalized in volume by nanoliposomes based on plant and marine lecithins, and then characterizes their properties by various physicochemical techniques. Firstly, the main fatty acid compositions of lecithins was analyzed by gas chromatography, secondly the stability of nanoliposomes and nanoliposomes/chitosan blends was determined by zetasizer, tensiometer, Transmission Electron Microscopy and rheometer. Finally, different properties of chitosan and the nanoliposomes/chitosan blend thin films were characterized by water contact angle, Fourier Transform Infrared Spectroscopy, Dynamic-Mechanical Thermal Analysis, Wide-Angle X-ray Scattering and Scanning Probe Microscopy in HarmoniX™ mode. From these experiments, the influences of nanoliposomes on thin films wettability, morphology, viscosity, mechanical properties and structural alteration were determined. The addition of nanoliposomes to chitosan and resulting nanoliposomes/chitosan blend thin films provides greater possibility of producing new materials for potential tissue engineering application.

1. Introduction

Chitosan is obtained by deacetylation of its parent polymer chitin, a polysaccharide widely distributed in nature (Muzzarelli et al., 2012). Its excellent biocompatibility, biodegradability, atoxicity, antibacterial and hemostatic properties, assure its useful applications in the field of tissue engineering, drug delivery, and gene therapy; in fact chitins and chitosans are non-allergenic drug carriers (Muzzarelli, 2010) whose safety has been amply assessed (Kean & Thanou, 2010). The physicochemical, structural, thermal, mechanical, biological and rheological properties of this polymer vary significantly with its molecular weight (Nguyen, Winnik, & Buschmann, 2009) and the degree of acetylation (Dash, Chiellini, Ottenbrite, & Chiellini, 2011).

In Tissue Engineering, the functional extracellular matrix production can be emulated to supply cells, which are suitable for biochemical environment *in situ* by functionalizing biomaterials with encapsulated bioactive molecules. In a broad sense, nanoliposomes share the same chemical structural and thermodynamic properties with liposome. However, compared to liposomes, nanoliposomes provide more surface area and have the potential to increase solubility, enhance bioavailability, improve controlled release and enable precision targeting of the encapsulated material to a greater extent (Mozafari, 2010). The main constituents of nanoliposomes are phospholipids, which are amphiphilic molecules containing water soluble, hydrophilic head section and a lipid-soluble, hydrophobic tail section. The good biocompatibility of phospholipids makes nanoliposomes an ideal carrier system with applications in different fields including food, cosmetics, pharmaceutics and tissue engineering (Mozafari, 2010; Nirmala et al., 2011).

Our nanoliposomes were prepared based on soya, rapeseed and marine lecithin, respectively, thus they were called soya/rapeseed/fish nanoliposomes. Rapeseed and soya lecithins consist mainly of three mono- and poly-unsaturated fatty acids namely oleic (C18:1), linoleic (C18:2), and linolenic acids (C18:3). Linoleic and linolenic acids are considered essential fatty acids because they are important to human health and our body cannot synthesize them (Coonrod, Brick, Byrne, DeBonte, & Chen, 2008). Marine lecithin from salmon (*Salmo salar*) contains a high percentage of polyunsaturated fatty acids (PUFAs), especially eicosapentaenoic acid (EPA, 20:5n-3) and docosahexaenoic acid (DHA, 22:6n-3) (Belhaj, Arab Tehrany, & Linder, 2010). Higher dietary PUFAs intakes are associated with reductions in the risk of

* Corresponding author. Tel.: +33 3 83 58 59 77; fax: +33 3 83 58 57 72.
E-mail address: elmira.arab-tehrany@ensaia.inpl-nancy.fr (E. Arab Tehrany).

0144-8617/$ – see front matter © 2012 Elsevier Ltd. All rights reserved.
doi:10.1016/j.carbpol.2012.01.007

cardiovascular disease, cancer, skeletal disorders, problems in pregnancy and child development, diabetes, central nervous system disorders, *etc.* (Mirajkar, Jamadar, Patil, & Mirajkar, 2011).

The aim of our work was to produce for the first time different nanoliposomes/chitosan blend thin films with a different range of proportion nanoliposomes, and to investigate the properties of these blend thin films relevant to tissue engineering applications, such as surface wettability, surface composition, mechanical and rheological properties, crystallinity and morphologies, in order to achieve a series of biomaterials which are more suitable for tissue regeneration applications.

2. Materials and methods

Chitosan sample (prepared from shrimp shells, practical grade) of deacetylation degree (DD) up to 75% was supplied by Sigma–Aldrich (Ref.: 417963, low molecular weight, viscosity >200 cP). The salmon lecithin from *S. salar*, rapeseed and soya lecithins were extracted by enzymatic hydrolysis. The lipids were extracted by use of a low temperature enzymatic process without any organic solvent (Linder, Matouba, Fanni, & Parmentier, 2002). BF_3 (boron trifluoride)/methanol (purity = 99%) and hexane (purity = 97%) used for CPG were purchased from Sigma–Aldrich (France) and Fisher (France). These organic solvents were analytical grade reagents. Acetic acid (100%) was supplied by Prolabo-VWR.

2.1. Preparation of nanoliposomes

The first time, we added 2 g of each lecithin into 38 mL of distilled water to obtain a solution with 5% (w/w) lecithin. The suspension mixed for 4 h under agitation in inert atmosphere (nitrogen). Then, we sonicated the mixture at 40 kHz and 40% power for 180 s (1 s on and 1 s off) to obtain the colloid suspension. Nanoliposomes samples were stored in sterilized bottles in the dark at 37 °C.

2.2. Characterization of nanoliposomes

2.2.1. Fatty acid composition

Fatty acid methyl esters (FAMEs) were prepared as described by Ackman (1998). The separation of the FAMEs was carried out using a Perichrom™ 2000 gas chromatograph (Perichrom, Saulx-lès-Chartreux, France), equipped with a flame-ionization detector. A fused silica capillary column was used (50 m, 0.25 mm inner diameter × 0.25 μm thin film thicknesses, CP 7419 Varian, Middelburg, Netherlands). Injector and detector temperatures were set at 260 °C. A column temperature was initially set at 145 °C for 5 min, then raised to 210 °C at a rate of 2 °C/min and held at 210 °C for 10 min. Standard mixtures (PUFA1 from marine source and PUFA2 from vegetable source; Supelco, Sigma–Aldrich, Bellefonte, PA, USA) were used to identify fatty acids. The results were presented as triplicate analyses.

2.2.2. Lipid classes

The lipid classes of the different fractions were determined by Iatroscan MK-5 Thin Layer Chromatography coupled with Flame Ionization Detector (TLC-FID, Iatron Laboratories Inc., Tokyo, Japan). Each sample was spotted on 10 Chromarod S-III silica coated quartz rods held in a frame. The rods were developed over 20 min in hexane/diethyl ether/formic acid (80:20:0.2, v/v/v), then oven dried for 1 min at 100 °C and finally scanned in the Iatroscan analyzer. The Iatroscan was operated under the following conditions: flow rate of hydrogen, 160 mL/min; flow rate of air, 2 L/min. A second migration using a polar eluent of chloroform, methanol, and ammoniac (65:35:5, v/v/v) made it possible to identify polar lipids. The FID results were expressed as the mean value of 10 separate samples. The following standards were used to identify the sample components:

- Neutral lipids: 1-monostearoyl-rac-glycerol, 1,2-dipalmitoyl-snglycerol, tripalmitin, cholesterol.
- Phospholipids: L-a-phosphatidylcholine, 3-sn-phosphatidylethanolamine, L-a-phosphatidyl-L-serine, L-a-phosphatidylinositol, lyso-phosphatidylcholine, sphingomyelin.

All standards were purchased from Sigma (Sigma–Aldrich Chemie GmbH, Germany). The recording and integration of the peaks were provided by the ChromStar internal software.

2.2.3. Nanoliposomes size measurement

The various nanoliposomes sizes were analyzed by dynamic light scattering using a Malvern Zetasizer Nano ZS (Malvern instruments, UK). The apparatus was equipped with a 4 mW He/Ne laser emitting 633 nm, measurement cell, photomultiplier and correlator. The samples were diluted in ultra-filtrate distilled water (1:400) and were placed in vertical cylindrical cells (10 mm diameters). The scattering intensity was measured at a scattering angle of 173° relative to the source using an avalanche of photodiode detector, at 25 °C. Intensity autocorrelation functions were analyzed by a General Purpose Algorithm (integrated in the Malvern Zetasizer software) in order to determine the distribution of the translational *z*-averaged diffusion coefficient of the particles, DT ($m^2\ s^{-1}$). The DT parameter is related to the hydrodynamic radius (R_h) of particles through the Stokes–Einstein relationship $DT = k_B T/(6\pi\eta R_h)$. During dispersion, particles are in a constant random Brownian motion, so it causes the intensity of scattered light to fluctuate as a function of time. Therefore, droplets sizes were obtained from the correlation function calculated by the dispersion technology software (DTS) using various algorithms. The refractive index (RI) and absorbance were fixed, respectively, at 1.471 and 0.01 at 25 °C. The measurements were carried out in five repetitions.

2.2.4. Electrophoretic mobility

Electrophoretic mobility measurements (μE) were performed by means of laser doppler electrophoresis. The sample was put in a standard capillary electrophoresis cell equipped with gold electrodes. The electrophoretic mobility of nanoliposomes was realized out to evaluate the surface net charge around lipid droplets. To avoid multiple scattering effects, the nanoliposomes were diluted with deionized water prior to analysis and then directly placed into the module. Measurements were performed directly in the diluted nanoliposomes and results were presented as triplicate analyses.

2.2.5. Transmission Electron Microscopy

Transmission Electron Microscopy (TEM) was employed to monitor the microstructure of nanoliposomes with a negative staining method. The nanoliposomes samples were diluted 10-folds with distilled water to reduce the concentration of the vesicles. Equal volumes of the diluted sample and a 2% ammonium molybdate solution were combined and left for 3 min at room temperature. A drop of this solution was placed on a Formvar-carbon coated copper grid (200 mesh, 3 mm diameter HF 36) for 5 min. The excess liquid was drawn off using filter papers. After drying the grid at room temperature for 5 min, micrographs were made using a Philips CM20 TEM operating at 200 kV and recorded using an Olympus TEM CCD camera (Colas et al., 2007).

2.2.6. Surface tension measurement

To test the stability of these nanoliposomes, three batches of each nanoliposomes, involving a total of 27 sets of nanoliposomes samples, were stored, respectively, at 4 °C, 25 °C and 40 °C. For

12 days, surface tension kinetics measurements of each sample (20 mL in 40 mL capped bottles) were measured using a Krüss K100 tensiometer (Germany). All the measurements were performed at a controlled temperature of 25 °C ± 0.5 °C.

2.3. Preparation of nanoliposomes/chitosan blends

2% (w/v) chitosan was dissolved in 1% acetic acid solution, and stirred overnight at room temperature and filtered through a sintered glass filter (Robu pore 1: pore between 100 and 160 μm) before being used. Then 5 mL, 10 mL and 20 mL of nanoliposomes solutions were added, respectively, to 95 mL, 90 mL and 80 mL chitosan solution (v/v) and stirred for 48 h to disperse nanoliposomes in chitosan solution.

2.3.1. Measuring system for the rheological behavior of pure chitosan and nanoliposomes/chitosan blend solutions

The time and temperature dependent storage modulus (G'), loss modulus (G'') and complex viscosity (η^*) were determined by Malvern Rheometer and Viscometer (Kinexus, UK), using a double gap concentric cylinder geometry (PL05) under a constant temperature of 25 °C. The specimens were loaded into the measuring geometry and left standing for 5 min to allow structure recovery and temperature equilibration. Each measurement was performed in triplicate.

2.4. Preparation of nanoliposomes/chitosan blend thin films

40 g of nanoliposomes/chitosan blend solution (according to Section 2.3) was casted in Teflon 90 mm × 110 mm Petri dishes (Welch, USA). The water was evaporated in an oven for 4 days at 37 °C. For a complete drying, the Petri dishes were kept in a hermetic container containing P_2O_5 powder. The final thin film thickness was 133 ± 10 μm measured by an electronic digital micrometer (0–25 mm, 1 μm) according to ASTM D 374-99.

2.5. Characterization methods of nanoliposomes/chitosan blend thin films

2.5.1. Contact angle measurement

Contact angle measurements of chitosan and nanoliposomes/chitosan blend thin films were performed by following the sessile drop method with a contact angle instrument (Digidrop Contact Angle Meter, France) equipped with an Image Analysis Attachment (Windrop, France). The probe liquids used were milli-Q water. Uniform drops of liquid (0.75 μl) were carefully deposited on the blend thin film surface using an assembly consisting of a micrometer syringe. The volume of the drops was kept constant since variations in the volume of the drops can lead to inconsistent contact angle measurements. Measurements were consistently conducted under the condition of 39% relative humidity and 23 °C. Contact angle measurements were recorded 15 times in three different locations on each side within 5 s for a given blend thin film.

2.5.2. Fourier Transform Infrared Spectroscopy

Fourier Transform Infrared Spectroscopy (FTIR) scans were obtained with a Tensor 27 mid-FTIR Bruker spectrometer (Bruker, Karlsruhe, Germany) equipped with a diamond ATR (Attenuated Total Reflectance) module specially design for thin films and a DTGS detector. Scanning rate was 20 kHz and 64 scans were used for reference and samples between 600 cm^{-1} and 4000 cm^{-1}. The nominal instrument resolution was 2 cm^{-1}. References were recorded in standard atmosphere. Then, the chitosan and nanoliposomes/chitosan blend thin films were put on the diamond crystal of the optical cell and a pressing was performed for thin film adsorption onto the crystal. Three to five separate experiments were done for each film. In addition, only the verso face was measured. All treatments were carried out using OPUS software (Bruker, Karlsruhe, Germany). Raw absorbance spectra were smoothed using a nine-points Savitsky-Golay smoothing functions. Elastic baseline correction using 200 points was then applied to spectra. After that, spectra were centered and normalized using OPUS software.

2.5.3. Dynamic Mechanical Thermal Analysis

The nanoliposomes/chitosan blend thin films were tested using a Dynamic Mechanical Thermal Analysis (DMTA) (Netzsch DMA 242 C analyzer) operating at 10 Hz, 3.33 Hz and 1 Hz frequency. The DMTA scan was performed between −100 °C and 200 °C with a heating rate of 2 °C/min. The specimens used were rectangular strips 5 mm wide, around 0.120 mm thick, and 30 mm in length. All measurements were repeated three times with each film system.

2.5.4. X-ray scattering

X-ray diffractograms were recorded by wide-angle X-ray scattering (WAXS). The selected tension and the intensity were 40 kV and 30 mA, respectively. The wavelength used was $K_{\alpha 1}$ copper radiation (λ = 0.154 nm), selected by means of a parabolic multilayer mirror (Osmic) and a cylindrical capillary. In this diffraction system (Inel, France), the sample axis (radial direction of the film) was perpendicular to the incident X-ray beam. The 2D transmission pattern was revealed with the adapted scanner (Fujifilm BAS 5000) with a maximum resolution of 25 μm, the image being readily obtained in digital form with a PC microcomputer. Subsequently, the diffraction curve, I (2θ), was analyzed using the PeakFit© software (SPSS Inc.) in view of extracting the different components: (i) background, (ii) crystalline peaks and, (iii) amorphous bump (amorphous 'halo'). The scan was taken in the 2θ range of 5–45° with step size of 0.029°. Crystallinity was determined the areas under the curves.

2.5.5. HarmoniX™ nanoscale material property mapping

Chitosan and nanoliposomes/chitosan blend thin films were characterized using Torsional Harmonic Atomic Force Microscopy analysis (TH-AFM) also called HarmoniX™ mode, a new dynamic mode technology, to assess the mechanical properties at a nanometric scale.

For HarmoniX™ mode, torsional harmonic cantilevers (HarmoniX™ probes, HMX, Brüker nanosurface) with resonance frequency 53 kHz and torsional frequency 951 kHz, and spring constant 1.2 N/m were used.

Measurements were done in air under ambient conditions at 37 °C using a Dimension 3100 with a NanoScopeV controller. For elastic modulus determination the cantilevers were calibrated using a standard PS/LDPE sample (Sahin, 2007).

Elasticity moduli were determined from DMT (Derjaguin–Muller–Toporov) model. The level of the force applied to the surface was adjusted by the amplitude set point, which was used for feedback control to 40% of the free amplitude. Imaging was performed at 0.5 Hz scan rate.

All offline image flattening and analyses were conducted with the software environment provided by the TH-AFM manufacturer. The statistical parameters related to sample roughness (ASME B46.1, 1995) were estimated by the equipment software including:

- average roughness (R_a): the average of absolute value of height deviations from mean surface;
- root mean square roughness (R_q): the root mean scare average of height deviations from the mean data plane;
- skewness (S_k): the measure of asymmetry of data or more precisely, the lack of symmetry (ISO 4287);
- kurtosis (E_k): the measure of amplitude distribution or more precisely the measure of whether the data are peaked or flat relative to a normal distribution.

3. Results and discussion

3.1. Lipid and nanoliposomes characterization

3.1.1. Fatty acid analyses

The main fatty acid composition is presented in this part. The percentage of total polyunsaturated fatty acids was the highest in soya lecithin, but, the variety of polyunsaturated fatty acids is higher in salmon lecithin. We observed nine polyunsaturated fatty acids of omega 3 and omega 6 in this lecithin.

The most significant proportions of fatty acids were C18:2(n-6), found in the polyunsaturated fatty acids class, C18:1(n-9) in the monounsaturated fatty acids class and C16:0 in the saturated fatty acids class for soya lecithin. The most important fatty acid was C18:1(n-9) with 55.78% for rapeseed lecithin in the monounsaturated fatty acid. The results show that the main percentage of C22:6(n-3) and C20:5(n-3) are in salmon lecithin compared to others unsaturated fatty acids with 10.78% and 6.71%, respectively.

3.1.2. Lipid classes

The lipid classes of lecithins were separated by thin-layer chromatography (Iatroscan). At that stage, salmon lecithin contains $38.9 \pm 0.8\%$ of triacylglycerols (TAG) and $61.1 \pm 0.2\%$ of polar fraction. Phosphatidylcholine (PC) thus represented the major class of phospholipids contained in salmon lecithin (33%). The percentages of polar fraction and TAG are $71.3 \pm 0.5\%$ and $28.7 \pm 0.1\%$, respectively, for rapeseed lecithin. The soya lecithin was found to be richer in polar lipids ($81.9 \pm 0.3\%$) than all other lecithins and that its TAG percentage was $18.2 \pm 0.2\%$.

3.1.3. Particle size analysis

The particle sizes of different nanoliposomes were measured immediately after sonication. The minimum achievable size generally depends on material viscosity and on applied sonication parameters (amplitude and time). In our study, the sizes of the nanoliposomes are presented in diameter. The average diameter of the nanoliposomes was 122 ± 3 nm and polydispersity index was 0.46 for particles from fish lecithin. The average diameter of the nanoliposomes for rapeseed and soya lecithin was 224 ± 14 nm and 138.5 ± 1 nm, respectively. Compared to fish lecithin, the polydispersity index was lower for rapeseed lecithin, with an index of 0.28, and for soya lecithin, with an index of 0.25. From our results, the percentage of mono and poly-unsaturated fatty acids varied according to the lecithin source. We observed that rapeseed lecithin contains an important percentage of mono-unsaturated fatty acids with 55.8% in comparison to soya and fish lecithins with 23.4% and 34.1%, respectively. An increased ratio of mono-unsaturated fatty acids consequently increased the size of the nanoliposomes. In addition, the ratio of long chain polyunsaturated fatty acids (LC-PUFAs) such as EPA and DHA changed the size of nanoliposomes. By increasing the LC-PUFAs ratio in lecithin, the size of nanoliposomes decreased and the polydispersity index increased. Thus, it was clear that the size of the nanoliposomes depended not only on such physical parameters as the amplitude of sonicator, but also on the composition of lecithin.

3.1.4. Electrophoretic mobility

Measurements of electrophoretic mobility vary between -3 and $-5\ \mu m\,cm/V\,s$ with a relatively high stability of the formulations. This is mainly due to the positive and negative charge brought by the polar fraction of lecithins (Section 3.1.2). According to the results obtained from zetasizer, the electrophoretic mobility is higher in soya lecithin ($-5\ \mu m\,cm/V\,s$) than for rapeseed ($-3.6\ \mu m\,cm/V\,s$) and fish ($-3.1\ \mu m\,cm/V\,s$) lecithins. One can notice that the value of electrophoretic mobility is negative throughout the storage period regardless of the type of formulation. The salmon, soya and rapeseed lecithins contain different types of phospholipids such as phosphatidylserine (PS), phosphatidic acid (PA), phosphatidylglycérol (PG), phosphatidylinositol (PI), phosphatidylethanolamine (PE), and PC. At physiological pH these phospholipids are negatively charged, except the PC which exhibits no global charge. Thus, these anionic fractions are probably responsible for the negative electrophoretic mobility (Chansiri, Lyons, Patel, & Hem, 1999). PC represented the major class of phospholipids contained in salmon lecithin (33%), rapeseed lecithin (29.8%) and soya lecithin (14.0%).

3.1.5. Transmission Electron Microscopy

Transmission Electron Microscopy (TEM) serves as visual information concerning the morphology. TEM images indicate that vesicles prepared by the sonicator method, are in the form of multilamellar vesicles (MLV) because of the sonication step. The bilayer nature of vesicles is clearly visible in these micrographs and confirms that the prepared lipid vesicles are actually nanoliposomes (Fig. 1). Also, we can observe some droplets in each formulation because of the presence of oil. The droplets in the three systems were found to be acceptable, even though there were some large droplets with a diameter greater than 200 nm.

3.1.6. Surface tension measurements of nanoliposomes

The surface tension ($\gamma_{surface}$) is an important tool for measuring the interaction capacity of the solvent with the polymer (Pillai, Paul, & Sharma, 2009). $\gamma_{surface}$ exists between the liquid phase and its saturated vapor in air.

These nanoliposomes which were stored at temperatures (4 °C, 25 °C and 40 °C) showed absolute stability during 12 days of storage. Fish nanoliposomes always showed a higher value of tension than the other two nanoliposomes. That is due to its higher polydispersity index than the other two nanoliposomes, according to Fowkes' studies (1964), because $\gamma_{surface}$ could be influenced by components dispersion, induction, dipole–dipole forces and hydrogen bonding (Erbil & Yildirim, 2006).

Nanoliposomes based on fish lecithin contain different types of PUFAs specifically, EPA and DHA. By increasing the concentration of PUFAs, the fluidity of the membrane increased and led to monolayer collapse at lower surface pressure or higher $\gamma_{surface}$. Rapeseed and soya lecithins have low $\gamma_{surface}$ due to the rigidity and the high-packing properties of saturated and mono-unsaturated fatty acids. Leshem, Landau, and Deutsch (1988) showed that the degree of unsaturation of sn-2 located in fatty acyl side-chains in typical membrane phospholipids has a remarkable effect on surface tension-associated parameters. For a fixed area monolayer in a completely expanded state, an increase in the number of *cis* double bonds was found to cause a concomitant increase in surface tension.

3.2. Stability measurements of pure chitosan and nanoliposomes/chitosan blend solutions

The intrinsic viscosity of the chitosan and nanoliposomes/chitosan samples used in this study was measured at 25 °C.

Measurements of the viscosity (η^*) as a function of the shear rate ($\gamma_{viscosity}$) are plotted for all the samples in Fig. 2. Rheological properties of chitosan and nanoliposomes/chitosan were determined using the rheometer and showed a shear thinning behavior.

The plots of chitosan aqueous solution, soya and rapeseed nanoliposomes/chitosan blend solutions show a shear thinning behavior and pseudoplastic characteristic, but the fish nanoliposomes/chitosan blend solution shows a shear thickening behavior at the beginning, and levels out around the shear rate of $0.5\ s^{-1}$.

Also, we can observe that when the shear rate is $5.14\ s^{-1}$, among the four systems the viscosity is highest in the chitosan

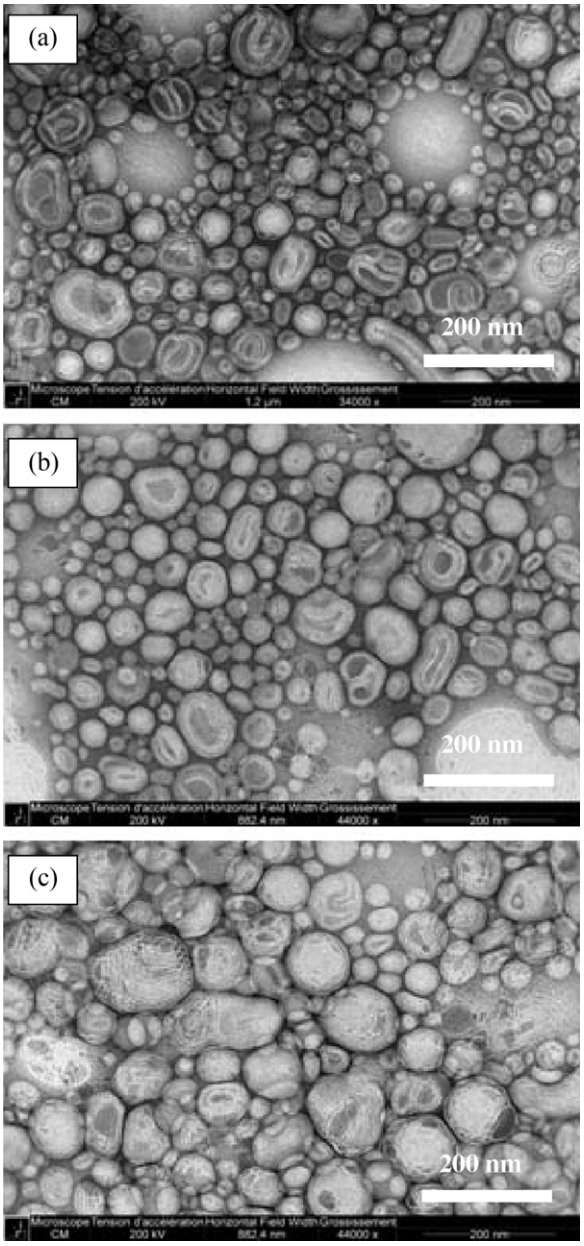

Fig. 1. Transmission Electron Microscopy (TEM) images of rapeseed (a), soya (b) and fish (c) nanolipomes.

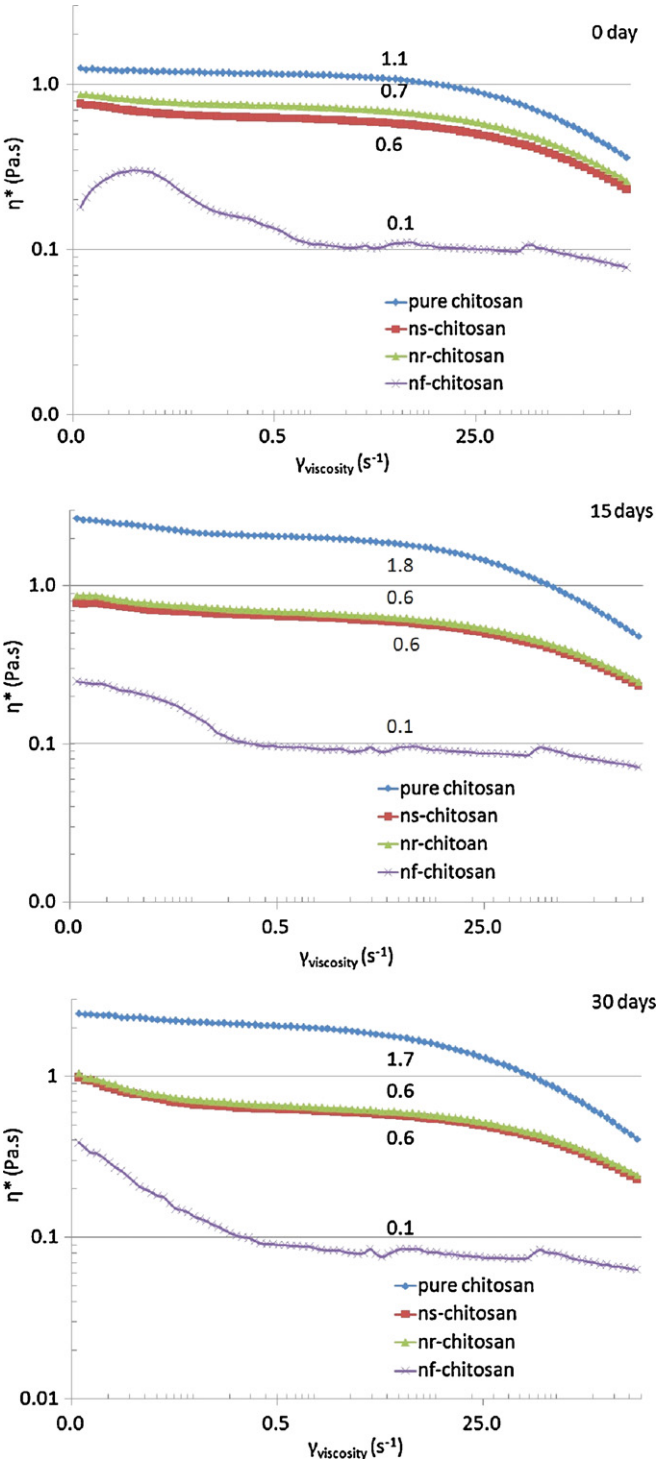

Fig. 2. Viscosity (η^*) *vs.* shear rate ($\gamma_{viscosity}$) for chitosan aqueous solutions and nanoliposomes/chitosan blend solutions at 0 day, 15 days and 30 days. Pure chitosan, soya nanoliposomes (ns-chitosan), rapeseed nanoliposomes (nr-chitosan), and fish nanoliposomes (nf-chitosan) blend thin films.

aqueous solution, lowest in the fish nanoliposomes/chitosan blend, and almost identical between the soya and rapeseed nanoliposomes/chitosan blend. The modification in the fish nanoliposomes/chitosan blend is due to the presence of higher amount of polyunsaturated fatty acids, especially, DHA and EPA in the fish lecithin which increase the fluidity of blend solution.

Madrigal-Carballo et al. (2008) showed that lecithin in solution often tends to form supramolecular assembly such as micelles, bilayer sheets and vesicles. Bilayers sheets can become a lamellar phase by being periodically stacked. Under certain conditions, multilamellar vesicles may become dispersed. Rheological properties of such dispersions will depend on the dynamic properties of the lamellar sheets (Alvarez, Seyler, Madrigal-Carballo, Vila, & Molina, 2007) or the multilamellar vesicles. A wide study about the rheopectic behavior (Alvarez et al., 2007; Manconi et al., 2005) of lecithin dispersions found in previous studies led to the conclusion that this characteristic corresponds to the transition from the lamellar phase of planar sheets to closed-structure morphology such as vesicles.

3.3. Characterization of chitosan and nanoliposomes/chitosan blend thin films

3.3.1. Contact angle measurements

The surface wettability of nanoliposomes/chitosan blend thin film was measured by contact angle analysis using water. The

Table 1
Water contact angle and surface energy of pure chitosan and nanoliposomes/chitosan blend thin films: soya nanoliposomes (ns-CS), rapeseed nanoliposomes (nr-CS), and fish nanoliposomes (nf-CS).

Equation of Owens–Wendt	Average of contact angle (°)		Total energy γ_T (MJ/m^2)	Polar component γ_p (MJ/m^2)	Dispersive component γ_d (MJ/m^2)
	Diiodomethane	Water			
Pure CS					
R	59.7 ± 1.0	109.5 ± 2.5	28.2	0	28.2
V	58.4 ± 2.7	101.3 ± 2.0	30.7	1.2	29.5
ns-CS 5%					
R	61.9 ± 3.1	102.6 ± 2.2	28.7	1.2	27.5
V	57.1 ± 2.1	100.4 ± 1.0	31.6	1.4	30.2
nr-CS 5%					
R	54.8 ± 2.7	95.7 ± 2.6	34.9	3.4	31.6
V	74.3 ± 4.3	95.1 ± 3.6	31.8	11.3	20.5
nf-CS 5%					
R	57.3 ± 1.3	98.9 ± 1.7	32.2	2.1	30.1
V	64.1 ± 0.1	87.9 ± 2.5	41.2	15.0	26.2
ns-CS 10%					
R	57.8 ± 1.3	85.5 ± 2.4	44.7	14.8	29.8
V	60.4 ± 2.7	82.4 ± 2.4	49.3	21.0	28.3
nr-CS 10%					
R	46.9 ± 2.5	75.0 ± 0.8	60.9	24.9	36.0
V	65.9 ± 3.9	68.8 ± 1.7	78.7	53.6	25.2
nf-CS 10%					
R	44.4 ± 2.7	71.6 ± 2.8	66.7	29.4	37.3
V	55.1 ± 0.7	64.2 ± 2.0	84.8	53.4	31.4
ns-CS20%					
R	62.7 ± 1.7	86.2 ± 0.9	56.1	29.1	27.0
V	29.3 ± 0.1	81.0 ± 1.9	66.4	21.9	44.5
nr-CS20%					
R	59.2 ± 0.7	81.0 ± 3.3	51.5	22.5	29.0
V	36.8 ± 1.6	73.2 ± 2.3	63.7	22.6	41.2
nf-CS 20%					
R	55.8 ± 0.7	66.6 ± 0.6	80.7	49.7	31.0
V	38.5 ± 1.7	52.1 ± 0.9	98.6	58.2	40.4

R – Recto, V – Verso, the value after "±" represents standard deviation.

contact angles of all the thin films are listed in Table 1. We did not observe the same wettability for the two sides. This difference is due to the nanoliposomes partial precipitation during water evaporation. Significant differences can be noticed in the surface wettability of blend thin film with varying proportions of nanoliposomes. The water contact angle of the 5% nanoliposomes blend thin films based on soya (100.4°), rapeseed (95.1°) and salmon (87.9°) is smaller than that of the pure chitosan film (101.3°). According to Table 1, the 10% and 20% nanoliposomes blend thin films are much smaller than that of the 5% nanoliposomes blend thin films. Among these results, we found that the fish nanoliposomes blend thin film contact angle decreased more compared with other films. This is likely due to its polar lipid proportion (part of lipid classes) and the amount of DHA and EPA. By increasing the amount of DHA and EPA, the fluidity parameter increases. In brief, the smaller value of the contact angle indicates the better surface wettability. When the amount of nanoliposomes is increased in the nanoliposomes/chitosan blend thin films; the water contact angle increases at the same time. Among all the thin films, fish nanoliposomes/chitosan blend thin films may be more suitable for tissue engineering application because of their polar components and polyunsaturated fatty acids.

3.3.2. Fourier Transform Infrared Spectroscopy

The Fourier Transform Infrared Spectroscopy (FTIR) spectra of chitosan and nanoliposomes/chitosan blend thin film are shown in Fig. 3 for comparative purposes.

Fig. 3 depicts the FTIR spectra of chitosan and the 10% nanoliposomes/chitosan blend thin films. From the pure chitosan spectrum, the carbonyl stretching (amide I band) at 1626 cm^{-1} and NH_2 bending (amide II band) at 1535 cm^{-1} could be clearly observed. The broad band ascribed to the stretching vibration of —NH_2 and —OH group appeared at 3000–3500 cm^{-1}, and the absorption bands at 1000–1200 cm^{-1} were attributed to its saccharine structure. The peaks around 2841 cm^{-1} and 2892 cm^{-1} are assigned to —CH_2 and —CH_3 groups (axial carbon–hydrogen bond). The sharp peaks at 1021 cm^{-1} and 1056 cm^{-1} correspond to indicate the C—O stretching vibrations (ν (C—O—C)). We can observe that wavenumbers assigned in the literature and those presented in this study, the difference does not exceed more than 20 cm^{-1}.

Compared with that of pure chitosan, the absorption band assigned to the stretching vibration of —CH_2— at 2921 cm^{-1} increased for nanoliposomes/chitosan blend thin films, and the amide II band shifted to 1545 cm^{-1} for all three blend thin films.

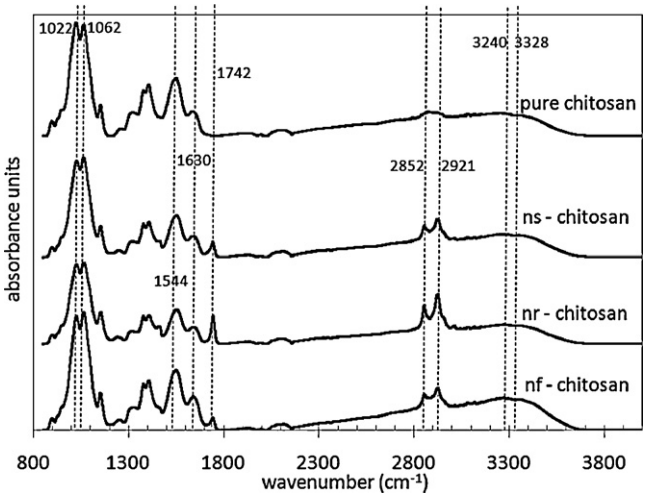

Fig. 3. FTIR spectrum of pure chitosan, soya nanoliposomes (ns-chitosan), rapeseed nanoliposomes (nr-chitosan), and fish nanoliposomes (nf-chitosan) blend thin films.

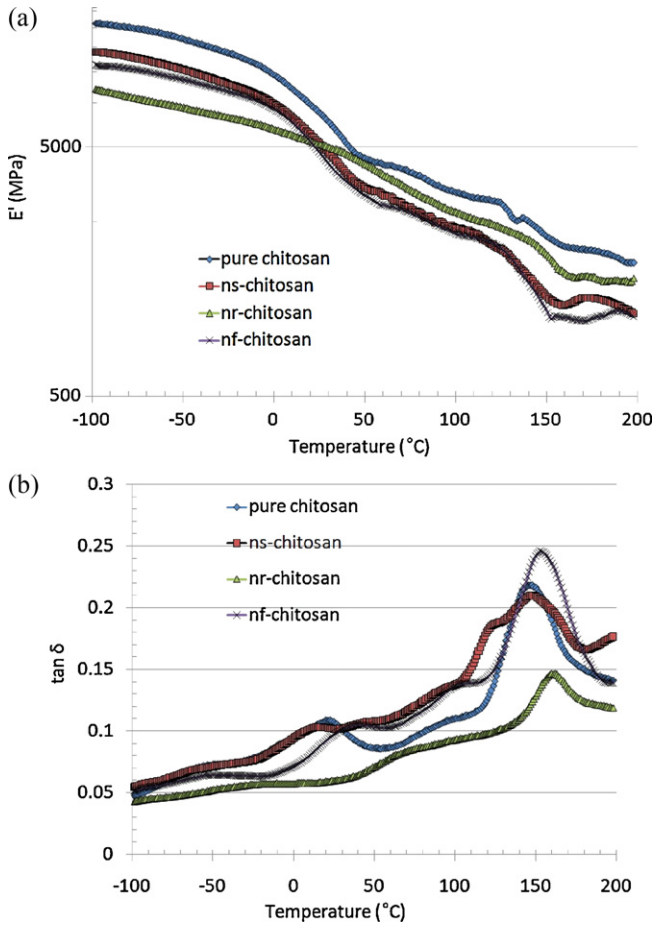

Fig. 4. Storage modulus (a) and tan δ (b) of pure chitosan, soya nanoliposomes (ns-chitosan), rapeseednanoliposomes (nr-chitosan), and fish nanoliposomes (nf-chitosan) blend thin films in the frequency of 10 Hz.

Although the amide I band had almost no shift. Moreover, the intensity of the peaks at 1021 cm^{-1}; 1052 cm^{-1}; and 1544 cm^{-1} appears to have decreased for soya nanoliposomes and rapeseed nanoliposomes blend thin films, and had almost no shift for the fish nanoliposomes/chitosan blend thin film. The intensity of the peaks at 1630 cm^{-1} appears to have decreased for soya nanoliposomes and rapeseed nanoliposomes blend thin films, and increased for the fish nanoliposomes/chitosan blend thin film. Furthermore, the intensity of the peaks at 2852 cm^{-1} and 2921 cm^{-1} show an increase for all three nanoliposomes/chitosan blend thin films. The intensity of the peaks between 3000 cm^{-1} and 3700 cm^{-1} appears to have decreased for the rapeseed nanoliposomes blend thin film, increased for the fish nanoliposomes blend thin film, and had almost no shift for the soya nanoliposomes blend thin film. In brief, the results indicated that some interaction have occurred between NH_2 groups of chitosan and nanoliposomes.

3.3.3. Dynamic Mechanical Thermal Analysis

Viscoelastic properties were observed using Dynamic Mechanical Thermal Analysis (DMTA) system. DMTA is a technique that is helpful for estimating the increase in stiffness of the composites caused by the adding of filler. As far as the relaxation behavior is concerned, DMTA is a more highly sensitive technique than Differential Scanning Calorimetry (DSC) to determine glass transition temperature T_g (Malheiro, Caridade, Alves, & Mano, 2010).

Fig. 4 shows the plots of the storage modulus (E') and the loss factor (tan δ) according to the temperature for our thin films at 10 Hz. A broad temperature range was used in order to cover the entire range of relaxation found in the literature (Mucha & Pawlak, 2005; Neto et al., 2005; Quijada-Garrido, Iglesias-Gonzalez, Mazon-Arechederra, & Barrales-Rienda, 2007; Toffey, Samaranayake, Frazier, & Glasser, 1996). It was observed that after heating, the samples presented a dark yellow coloration indicating that the heating had caused degradation of chitosan molecules.

Table 2
Dynamic mechanical relaxations of chitosan and nanoliposomes/chitosan blend thin films at a series of frequencies, Young's modulus of chitosan and nanoliposomes/chitosan blend thin films at three temperatures (−18 °C, 25 °C and 37 °C): soya nanoliposomes (ns-CS), rapeseed nanoliposomes (nr-CS), and fish nanoliposomes (nf-CS) blend thin films.

	$T_{max} \equiv T_\alpha$	T_β	Young's modulus (GPa)		
			−18 °C	25 °C	37 °C
Pure CS	142.9	91.3	11.5	6.9	5.5
ns-CS	145.9	84.9	8.7	5.2	4.2
nr-CS	156.9	60.3	6.4	5.1	4.8
nf-CS	151.9	101.3	8.1	4.8	4.8

As shown in Fig. 4(a), the storage modulus of the chitosan blend thin film decreased with the introduction of nanoliposomes. Among all the blend thin films, the rapeseed nanoliposomes/chitosan blend film had the lowest value (0.85 GPa). Whereas the storage modulus of soya and fish nanoliposomes/chitosan blend thin films was between 1 and 1.2 MPa. Young's modulus (E) of pure chitosan and nanoliposomes/chitosan blend thin films was calculated at three temperatures (−18 °C, 25 °C and 37 °C) using the relation (Babak, Desbrières, & Tikhonov, 2005):

$$E^2 = E'^2 + E''^2$$

where E'' (loss modulus) was calculated using the relation $\tan\delta = E''/E'$ (shown in Table 2). The evolution of Young's modulus in relation to the temperature showed that the addition of nanoliposomes decreased Young's modulus of film compared to the pure chitosan thin film. The differences of Young's modulus were the highest in subzero temperatures (from 25% to 50% of pure chitosan thin film) and decreased at 37 °C (from 13% to 24% of pure chitosan thin film). Moreover, at a range of operate temperatures; the nanoliposomes seem to stabilize the Young's modulus (except for soya nanoliposomes) which can serve interest for tissue engineering applications.

Relaxation processes of nanoliposomes/chitosan blend thin films were measured by DMTA. For the pure chitosan thin film, at least three relaxations could be distinguished in Fig. 4(b) at 19 °C, 91 °C and 143 °C. We can see a maximum of tan δ at 143 °C corresponding to the α-relaxation, which could be attributed to the glass transition (T_g). Mucha and Pawlak (2005) reported that T_g of chitosan decreases with increasing deacetylation degree (DD). They found that T_g varied from 156 °C to 170 °C for the chitosan thin film with DD from 59% to 86%. Moreover, Lazaridou and Biliaderis (2002) and Quijada-Garrido, Iglesias-Gonzalez, Mazon-Arechederra, and Barrales-Rienda (2007) reported that the T_g was between 85 °C and 95 °C with a DD of about 90%. Thus, we can hypothesize that the DD of chitosan used in this work was around 86–90% (T_g = 143 °C). The second relaxation (91.3 °C) may be considered as a β-relaxation due to the presence of acetamide groups in chitosan as proposed by Wan, Lu, Dalai, and Zhang (2009) for a β-relaxation at 102 °C (pure chitosan, DD = 82.8%). The third relaxation at 19 °C could be a γ-relaxation due to the presence of phospholipids in our blends.

The addition of 10% nanoliposomes in chitosan film changes the T_g by either a strong or slight augmentation depending on the composition. The addition of fish and rapeseed nanoliposomes/chitosan shifted the T_g to 152 °C and 157 °C, respectively; whereas the soya nanoliposomes had a little effect on the T_g, with a temperature of 146 °C. Moreover, the rapeseed nanoliposomes/chitosan blend thin

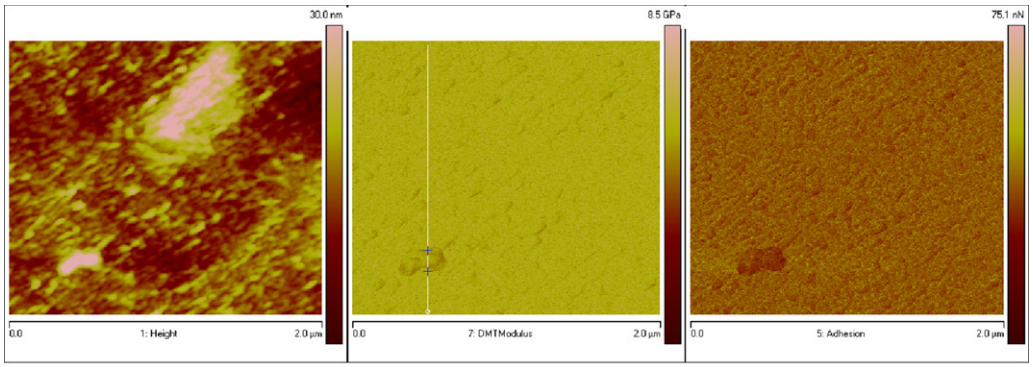

(a) Pure chitosan

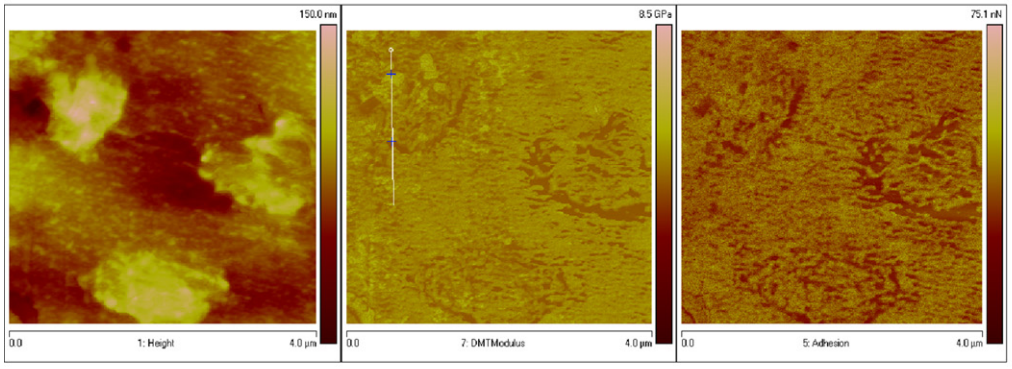

(b) soya nanoliposomes / chitosan

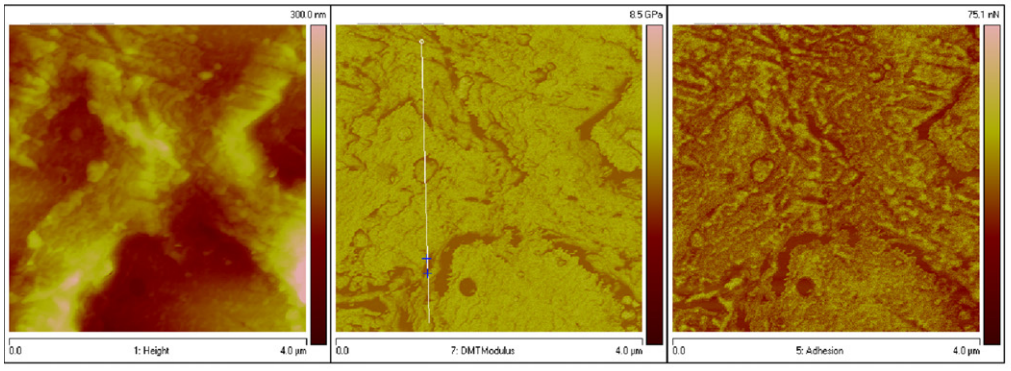

(c) rapeseed nanoliposomes / chitosan

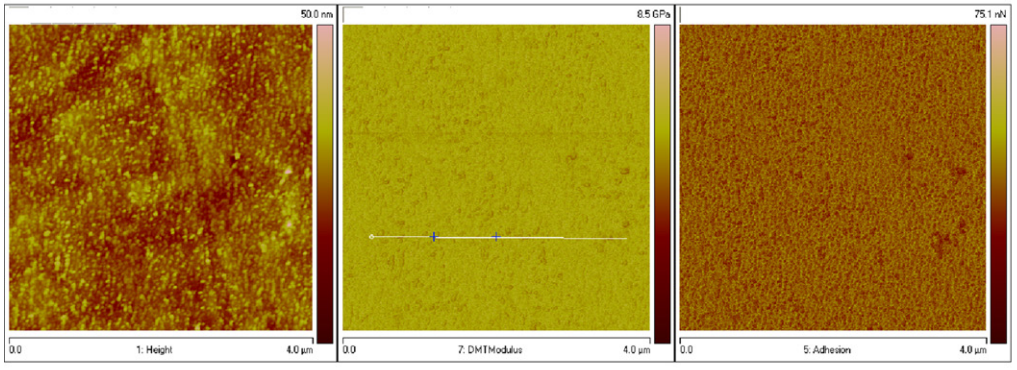

(d) fish nanoliposomes / chitosan

Fig. 5. TH-AFM images of pure chitosan (a), soya nanoliposomes/chitosan (b), rapeseed nanoliposomes/chitosan (c) and fish nanoliposomes/chitosan (d) thin film surfaces: height, DMT modulus and adhesion force.

film showed a lower viscous effect ($\tan\delta$) than the others. This shift was likely related to an interaction between chitosan and nanoliposomes. The authors can hypothesize that the colloid dispersion may have an effect on these shifts.

3.3.4. X-ray scattering

Many literatures (Baskar & Sampath Kumar, 2009; Chen, Wang, Mao, Liao, & Hsieh, 2008; Ikejima & Inoue, 2000; Peter et al., 2010; Zeng et al., 2009; Zhao et al., 2011) reported the degree of crystallinity of their chitosan studies, but no obvious peak was found in the diffractograms of our pure chitosan thin film, which indicates that our chitosan does not form its own crystalline region but maintains amorphous state during film formation. However, we have observed on X-ray spectra (not shown here) some slight peaks in the blend thin film around $2\theta = 19.09^\circ$ indicating some repeat bondings of phospholipids in the nanoliposomes, caused by the presence of certain elements (e.g. N, O, P). The adding of nanoliposomes in chitosan may break the hydrogen bonding between amino groups and hydroxyl groups in chitosan, which results in some repeat bonding structures of our blend thin film.

3.3.5. HarmoniX™ nanoscale material property mapping

Fig. 5 shows that the surface microstructure of films was drastically affected by adding nanoliposomes. The chitosan thin film (Fig. 5a) presents a homogenous smooth morphology with $R_a = 3.5$ nm and $R_q = 5$ nm. The soya nanoliposomes/chitosan surface (Fig. 5b) shows the presence of micro-domains. These micro-domain surfaces are associated with both a difference of mechanical properties and a particular structure of soya nanoliposomes. Compared with the chitosan thin film, the soya nanoliposomes/chitosan blend thin film had a higher roughness of 15 nm and 20 nm for R_a and R_q, respectively.

The nanomechanical properties of chitosan and nanoliposomes/chitosan blend thin films were characterized by HarmoniX™ mode. The results show that Young's modulus determined by DMT model in average on the surface of chitosan (around 1.55 GPa) and the fish nanoliposomes/chitosan (around 1.3 GPa) were more important than the soya (around 0.6 GPa) and rapeseed nanoliposomes/chitosan blend thin films (around 0.9 GPa).

The elastic modulus of a polymeric sample depends on the thermal history and the degree of cross-linking (Kocun, Grandbois, & Cuccia, 2011). A good correlation between the Young's modulus value obtained from HarmoniX™ stiffness data and the nominal Young's modulus values in the range of 4–5 GPa (at 37 °C) obtained by DMTA was compared for different systems (Sahin & Erina, 2008). Fig. 5 shows DMT images and elasticity profiles of different thin films. We can observe that the Young's modulus obtained by TH-AFM were smaller than the values obtained by DMTA. Indeed, the HarmoniX™ analysis is a surface measurement without considering of the distribution in volume of nanoliposomes whilst DMTA analysis is a volume measurement with the average effect of Young's modulus.

The adhesion images were also presented for chitosan and nanoliposomes/chitosan blend thin films in Fig. 5. In general, the measured values of adhesive force (F_{adh}) between surfaces include contributions from Van der Waals forces (F_{vdw}), electrostatic forces (F_e) and chemical bonding forces (F_b) (Lubarsky, Davison, & Bradley, 2004). The results show that adhesion force of the fish nanoliposomes/chitosan blend films was higher than chitosan with 16.4 nN and 15.5 nN, respectively. The soya and rapeseed nanoliposomes/chitosan blend thin films had a less important adhesion force than the pure chitosan film with 11.7 nN and 10.4 nN, respectively. The adhesion images showed lower tip-sample adhesion force (F_{adh}) between chitosan and the silicon tip. By adding nanoliposomes, we improved the adhesion force between the blend thin films and silicon-tip.

Compared to the chitosan thin film, the fish nanoliposomes/chitosan blend thin film had a similar roughness of 3 nm and 4 nm for R_a and R_q, respectively. By adding the rapeseed nanoliposomes to the chitosan film, the roughness parameters increased to 30 nm and 38 nm for R_a and R_q, respectively. Thus, in order to precisely define the effects of nanoliposomes on topographical parameters, it is necessary to follow the variation of complementary parameters, especially the profile symmetry/height balance, via both E_k and S_k parameters. Compared with the pure chitosan thin film ($S_k = 1$ nm and $E_k = 5$ nm), the adding of nanoliposomes to chitosan had an S_k less important with 0.3 nm, 0.4 nm, and 0.5 nm for the soya, rapeseed and fish nanoliposomes/chitosan blend thin films, respectively. We observed no significant variation for E_k. Thus, R_a, R_q, and S_k are the most important parameters in this study.

4. Conclusion

Three different nanoliposomes/chitosan blends were prepared, characterized and compared with corresponding chitosan scaffolds. The mechanical, rheological, morphological, structural properties and wettability of the scaffolds was significantly affected by the addition of different nanoliposomes. When nanoliposomes were added into the chitosan scaffold, the water contact angle of thin films decreased, which was related in an increase of wettability. The deformation of our blend thin films increased when given the same stress which showed a decrease of Young's modulus. We also found that the viscosity of our blend solutions decreased, shown by the results of the rheometer. From the X-ray diffractograms, we can see some slight peaks in blend thin films, which indicated some alterations of diffraction signature. Thus, nanoliposomes are expected to enhance the crystallinity degree of pure chitosan. However, the mechanical properties consistently present issues to be resolved after the adding of nanoliposomes. The morphological and nanomechanical properties and adhesion force of each scaffold system were determined by TH-AFM. The results obtained by TH-AFM showed that among nanoliposomes/chitosan blend thin films, the fish nanoliposomes/chitosan thin film has the most similar properties compared to the pure chitosan thin film.

Based on our results, cellular attachment and function on the pure chitosan thin films may be enhanced by adding nanoliposomes because of the increase of wettability related to nanoliposomes. The mechanical properties of nanoliposomes/chitosan blend thin films maintained in the same level as the chitosan thin film, which shows that the fish nanoliposomes/chitosan blend thin film is more suitable for bone tissue engineering application. Whereas the soya and the rapeseed nanoliposomes/chitosan blend thin film are more suitable for soft tissue engineering application.

Acknowledgement

We would like to thank Ms. Lauren Carmin for her advice and assistance in editing this paper.

References

Ackman, R. G. (1998). Remarks on official methods employing boron trifluoride in the preparation of methyl esters of the fatty acids of fish oils. *Journal of the American Oil Chemists' Society*, *75*, 541–545.

Alvarez, M. A., Seyler, D., Madrigal-Carballo, S., Vila, A. O., & Molina, F. (2007). Influence of the electrical interface properties on the rheological behavior of sonicated soy lecithin dispersions. *Journal of Colloid and Interface Science*, *309*, 279–282.

Babak, V. G., Desbrières, J., & Tikhonov, V. E. (2005). Dynamic surface tension and dilational viscoelasticity of adsorption layers of a hydrophobically modified chitosan. *Colloids and Surfaces A: Physicochemical and Engineering Aspects*, *255*, 119–130.

Baskar, D., & Sampath Kumar, T. S. (2009). Effect of deacetylation time on the preparation, properties and swelling behavior of chitosan film. *Carbohydrate Polymers*, *78*, 767–772.

Belhaj, N., Arab Tehrany, E., & Linder, M. (2010). Oxidative kinetics of salmon oil in bulk and in nanoemulsion stabilized by marine lecithin. *Process Biochemistry*, *45*, 187–195.

Chansiri, G., Lyons, R. T., Patel, M. V., & Hem, S. T. (1999). Effect of surface charge on the stability of oil/water emulsions during steam sterilization. *Journal of Pharmaceutical Sciences*, *88*, 454–458.

Chen, C. H., Wang, F. Y., Mao, C. F., Liao, W. T., & Hsieh, C. D. (2008). Studied of chitosan: Preparation and characterization of chitosan/poly (vinyl alcohol)/gelatin ternary blend films. *International Journal of Biological Macromolecules*, *43*, 37–42.

Colas, J. C., Shi, W., Rao, V. S. N. M., Omri, A., Mozafari, M. R., & Singh, H. (2007). Microscopical investigations of nisin-loaded nanoliposomes prepared by Mozafari method and their bacterial targeting. *Micron*, *38*, 841–847.

Coonrod, D., Brick, M. A., Byrne, P. F., DeBonte, L., & Chen, Z. (2008). Inheritance of long chain fatty acid content in rapeseed (*Brassica napus* L.). *Euphytica*, *164*, 583–592.

Dash, M., Chiellini, F., Ottenbrite, R. M., & Chiellini, E. (2011). Chitosan – A versatile semi-synthetic polymer in biomedical applications. *Progress in Polymer Science*, *36*, 981–1014.

Erbil, H., & Yildirim. (2006). *Surface chemistry of solid and liquid interfaces*. Oxford: Blankwell Publishing Ltd., p. 332.

Fowkes, F. M. (1964). Ideal two - dimensional solutions. IV. Penetration of monolayers of polymers. *Journal of Physical Chemistry*, *68*, 3515–3520.

Ikejima, T., & Inoue, Y. (2000). Crystallization behavior and environmental biodegradability of the blend films of poly (3-hydroxybutyric acid) with chitin and chitosan. *Carbohydrate Polymers*, *41*, 351–356.

Kean, T., & Thanou, M. (2010). Biodegradation, biodistribution and toxicity of chitosan. *Advanced Drug Delivery Reviews*, *62*, 3–11.

Kocun, M., Grandbois, M., & Cuccia, L. A. (2011). Single molecule atomic force microscopy and force spectroscopy of chitosan. *Colloids and Surfaces B*, *82*, 470–476.

Lazaridou, A., & Biliaderis, C. G. (2002). Thermophysical properties of chitosan, chitosan-starch and chitosan-pullulan films near the glass transition. *Carbohydrate Polymers*, *48*, 179–190.

Leshem, Y., Landau, E., & Deutsch, M. (1988). A monolayer model study of surface tension-associated parameters of membrane phospholipids: Effect of unsaturation of fatty acyl tails. *Journal of Experimental Botany*, *39*, 1679–1687.

Linder, M., Matouba, E., Fanni, J., & Parmentier, M. (2002). Enrichment of salmon oil with n-3 PUFA by lipolysis, filtration and enzymatic re-esterification. *European Journal of Lipid Science and Technology*, *104*, 455–462.

Lubarsky, G. V., Davison, M. R., & Bradley, R. H. (2004). Elastic modulus, oxidation depth and adhesive force of surface modified polystyrene studied by AFM and XPS. *Surface Science*, *558*, 135–144.

Madrigal-Carballo, S., Seyler, D., Manconi, M., Mura, S., Vila, A. O., & Molina, F. (2008). An approach to rheological and electrokinetic behaviour of lipidic vesicles covered with chitosan biopolymer. *Colloids and Surfaces A: Physicochemical Engineering Aspects*, *323*, 149–154.

Malheiro, V. N., Caridade, S. G., Alves, N. M., & Mano, J. F. (2010). New poly (ε-caprolactone)/chitosan blend fibers for tissue engineering applications. *Acta Biomaterialia*, *6*, 418–428.

Manconi, M., Aparicio, J., Seyler, D., Vila, A. O., Figueruelo, J., & Molina, F. (2005). Effect of several electrolytes on the rheopectic behaviour of concentrated soy lecithin dispersions. *Colloids and Surfaces A: Physicochemical and Engineering Aspects*, *270*, 102–106.

Mirajkar, R. N., Jamadar, S. A., Patil, A. V., & Mirajkar, S. N. (2011). Omega-3 fatty acids - Clinical implications. *International Journal of ChemTech Research*, *3*, 724–732.

Mozafari, M. R. (2010). Nanoliposomes: preparation and analysis. *Methods in molecular biology*, *605*, 29–50.

Mucha, M., & Pawlak, A. (2005). Thermal analysis of chitosan and its blends. *Thermochimica Acta*, *427*, 69–76.

Muzzarelli, R. A. A. (2010). Chitins and chitosans as immunoadjuvants and non-allergenic drug carriers. *Marine Drugs*, *8*, 292–312 (Review).

Muzzarelli, R. A. A., Boudrant, J., Meyer, D., Manno, N., DeMarchis, M., & Paoletti, M. G. (2012). Current views on fungal chitin/chitosan, human chitinases, food preservation, glucans, pectins and inulin: A tribute to Henri Braconnot, precursor of the carbohydrate polymers science, on the chitin bicentennial. *Carbohydrate Polymers*, *87*, 995–1012.

Neto, C. G. T., Giacometti, J. A., Job, A. E., Ferreira, F. C., Fonseca, J. L. C., & Pereira, M. R. (2005). Thermal analysis of chitosan based networks. *Carbohydrate Polymers*, *62*, 97–103.

Nguyen, S., Winnik, F. M., & Buschmann, M. D. (2009). Improved reproducibility in the determination of the molecular weight of chitosan by analytical size exclusion chromatography. *Carbohydrate Polymers*, *75*, 528–533.

Nirmala, R., Park, H.-M., Navamathavan, R., Kang, H.-S., El-Newehy, M. H., & Kim, H. Y. (2011). Lecithin blended polyamide-6 high aspect ratio nanofiber scaffolds via electrospinning for human osteoblast cell culture. *Materials Science and Engineering C*, *31*, 486–493.

Peter, M., Binulal, N. S., Soumya, S., Nair, S. V., Furuike, T., Tamura, H., et al. (2010). Nanocomposite scaffolds of bioactive glass ceramic nanoparticles disseminated chitosan matrix for tissue engineering applications. *Carbohydrate Polymers*, *79*, 284–289.

Pillai, C. K. S., Paul, W., & Sharma, C. P. (2009). Chitin and chitosan polymers: Chemistry, solubility and fiber formation. *Progress in Polymer Science*, *34*, 641–678.

Quijada-Garrido, I., Iglesias-Gonzalez, V., Mazon-Arechederra, J. M., & Barrales-Rienda, J. M. (2007). The role played by the interactions of small molecules with chitosan and their temperatures. Glass-forming liquids: 1,2,3-Propantriol (glycerol). *Carbohydrate Polymers*, *68*, 173–186.

Sahin, O. (2007). Harnessing bifurcations in tapping-mode atomic force microscopy to calibrate time-varying tip sample force measurements. *Review of Scientific Instruments*, *78*, 103707–103711.

Sahin, O., & Erina, N. (2008). High-resolution and large dynamic range nanomechanical mapping in tapping-mode atomic force microscopy. *Nanotechnology*, *19*, 445717–445725.

Toffey, A., Samaranayake, G., Frazier, C. E., & Glasser, W. G. (1996). Chitin derivatives. I. Kinetics of the heat-induced conversion of chitosan to chitin. *Journal of Applied Polymer Science*, *60*(1), 75–85.

Wan, Y., Lu, X., Dalai, S., & Zhang, J. (2009). Thermophysical properties of polycaprolactone/chitosan blend membranes. *Thermochimica Acta*, *487*, 33–38.

Zeng, R., Tu, M., Liu, H. W., Zhao, J. H., Zha, Z. G., & Zhou, C. R. (2009). Preparation, structure, drug release and bioinspired mineralization of chitosan-based nanocomplexes for bone tissue engineering. *Carbohydrate Polymers*, *78*, 107–111.

Zhao, J. H., Han, W. Q., Chen, H. D., Tu, M., Zeng, R., Shi, Y. F., et al. (2011). Preparation, structure and crystallinity of chitosan nano-fibers by a solid–liquid phase separation technique. *Carbohydrate Polymers*, *83*, 1541–1546.